Analyst

PAPER

View Article Online
View Journal

Cite this: DOI: 10.1039/d5an01290b

Targeted screening of natural thrombin inhibitors from herbal extracts using an enzyme-immobilized microfluidic reactor

Xian-Na Wang, Ji Zhang, Yahui Song, Rui-Ping Song, Weiwei Tang* and Bin Li *

An enzyme-immobilized microfluidic reactor (EIMR) is a highly efficient platform for *in vitro* screening of catalysts and inhibitors. Herein, an EIMR integrated in a glass-PDMS hybrid microfluidic chip (HMC) was developed for *in situ* screening of potential thrombin inhibitors from complex herbal extracts. Thrombin was selectively immobilized *in situ* on a gold nanoparticle-functionalized porous silica film (AuNPs@FPSF)-coated ITO glass slide using the DNA aptamer TBA_{15}, while the microfluidic part of the EIMR, comprising a microchannel and microfluidic connections, was formed in a polydimethylsiloxane (PDMS) plate. The EIMR was compatible with dual-model detection: fluorescence analysis and matrix-assisted laser desorption/ionization mass spectrometry (MALDI MS). A customized fluorescent substrate was synthesized for *in situ* monitoring of the thrombin reaction using fluorescence microscopy, and its enzymatic hydrolysate was detected and quantified using MALDI MS. The reproducibility of the EIMR was significantly improved by optimizing conditions for thrombin immobilization and the concentration of a fluorescent substrate. As a result, eight potential thrombin inhibitors were discovered from five herbal extracts, and their inhibitory activities were determined using MALDI MS. Overall, the developed EIMR exhibited the advantages of high sensitivity, ease of use, and fast-response, facilitating the screening of candidate enzyme inhibitors from complex herbal plants.

Received 7th December 2025,
Accepted 5th February 2026

DOI: 10.1039/d5an01290b

rsc.li/analyst

1. Introduction

Cardiocerebrovascular disease is a serious threat to human beings, characterized by high prevalence, high rates of disability, and high mortality. Aging populations, economic development, and lifestyle changes contribute to the rising prevalence of cardiocerebrovascular disease, highlighting the urgent need for effective treatment options.[1] Thrombin, a key enzyme involved in blood coagulation and platelet aggregation, is of fundamental importance in maintaining normal hemostatic function.[2,3] Thrombin is widely distributed in the vascular system and is involved in multiple pathological processes, such as stroke, thrombosis, blood clotting, cancer invasion, and neurodegenerative diseases.[4] It has become a crucial target of multiple cardiocerebrovascular disease therapies because of its central role in the coagulation cascade.[5,6] When a blood vessel is damaged, inactive zymogen prothrombin is rapidly converted to thrombin, resulting in a large variation in the thrombin concentration during a coagulation reaction.[7] Anti-thrombin therapy is one of the most effective strategies for the prevention and treatment of cardiocerebrovascular diseases.[8] Therefore, efforts have been made to discover novel, highly efficient thrombin inhibitors with low toxicity, especially sourced from natural products.

Herbal plants contain a large pool of bioactive compounds, which show high potential in preventing cardiocerebrovascular diseases.[9–11] Considerable attention has been paid to the development of various methods for the rapid *in vitro* screening of natural products with cardio- and cerebrovascular protective activities. Generally, extraction, fractionation, purification, structure identification, and activity determination are the basic components involved in traditional screening methods. However, these methods have several limitations, such as labor-intensive operation, non-targeted screening, and low efficiency.[12,13] Owing to its specificity toward a particular substrate and high catalytic efficiency, the enzyme immobilization strategy has been successfully employed for the rapid discovery of active natural products from herbal extracts.[14,15] However, conventional techniques for enzyme immobilization suffer from suboptimal recovery of *in vitro* biological activity due to insufficient enzyme loading and inadequate stability.[16,17] In contrast, an enzyme-immobilized microfluidic reactor (EIMR), which involves the use of microfluidic chips for enzyme immobilization, has attracted significant attention

State Key Laboratory of Natural Medicines and School of Traditional Chinese Pharmacy, China Pharmaceutical University, Nanjing, 210009, China.
E-mail: weiweitang@cpu.edu.cn, binli@cpu.edu.cn

due to its ability to precisely control immobilization parameters, resulting in immobilized enzymes with high activity and stability.[18,19] In combination with the additional benefits of miniaturization, heterogeneous catalysis, and flow-mode operation, this technique represents a promising alternative screening option for enzyme inhibitors.[20] Moreover, an EIMR is compatible with multiple analytical modalities, such as chromatography, electrophoresis, fluorescence, and mass spectrometry (MS), for biomedical, pharmaceutical, and proteomic studies.[21–23]

Nevertheless, current microfluidic-based screening systems still face critical technical challenges. Fluorescence analysis plays an important role in enzyme inhibitor screening due to its high sensitivity, real-time monitoring capability, high throughput, and non-invasiveness.[24] However, the limited selectivity of fluorescence spectroscopy and possible spontaneous fluorescence or fluorescence quenching (*e.g.*, flavonoids and anthraquinones) may lead to false-positive or false-negative results.[25] Matrix-assisted laser desorption/ionization mass spectrometry (MALDI MS) serves as a valuable supplement to fluorescence analysis, enabling *in situ* analysis of complex samples and exhibiting advantages such as superior mass resolution, salt tolerance, resistance to contamination, and high compatibility.[26,27] MALDI MS can be integrated with microfluidic chips to facilitate the rapid discovery and identification of active compounds in herbal extracts.[28] The dual-signal mode based on fluorescence and MALDI MS can minimize the occurrence of false-positive or false-negative results to improve the reproducibility and accuracy of candidate drug screening.

In this work, a hybrid microfluidic chip (HMC) was developed, which was made of an AuNPs-functionalized porous silica film (AuNPs@FPSF)-coated indium tin oxide (ITO) glass slide and polydimethylsiloxane (PDMS) plate with a microchannel array. The DNA aptamer TBA_{15} was immobilized on the HMC *via* an Au–S bond for thrombin immobilization. After sequentially infusing herbal extracts and the fluorescence substrate of thrombin into the channels, the thrombin reaction was monitored *via* fluorescence microscopy. The channels were subsequently analyzed *via* MALDI MS to quantify the thrombin hydrolysate. Ultimately, eight potential thrombin inhibitors were found and identified in five herbal extracts. It is an efficient screening method for the "fishing and detection" of candidate thrombin inhibitors from herbal extracts.

2. Experimental

2.1. Preparation of HMC

The porous silica film (PSF)-coated ITO glass slide was synthesized using a modified Stöber-solution growth approach.[29] Initially, 0.24 g of cetyltrimethylammonium bromide (CTAB) was dissolved in 105 mL of deionized water and mixed with 42 mL of ethanol. A 125 μL ammonia aqueous solution (25 wt%) and 200 μL tetraethoxysilane (TEOS) were then added dropwise under vigorous stirring. After thorough mixing, the freshly cleaned ITO glass slide was immersed in the solution under quiescent condition at 60 °C in a water bath. The silica film was formed on the ITO glass slide after 24 h. The modified ITO glass slide was rinsed thoroughly with water and aged at 100 °C overnight. The CTAB surfactants in the silica nanochannels were removed by immersing the ITO glass slide in 0.1 M HCl–ethanol solution under moderate stirring for 15 min. The PSF-coated ITO glass slide was thoroughly rinsed with ethanol and aged at 80 °C for 2 h, which was used as a hard template to support the AuNPs. A quaternary amino (R_4N^+) functionalized PSF-coated ITO glass slide was prepared by immersing the slide in an acetone solution containing 1% N-trimethoxysilylpropyl-N,N,N-trimethylammonium chloride (TMAC) (v/v) for 2 h under magnetic stirring at room temperature and then rinsing it with acetone, ethanol, and water in sequence. After aging at 80 °C for 2 h, the FPSF-coated ITO glass slide was immersed in a 5 mM $HAuCl_4$ solution for 8 h under stirring at room temperature, followed by rinsing with water and immersion in 0.1 M $NaBH_4$ with ice bath cooling for 2 h. Finally, an AuNPs@FPSF/ITO glass was achieved upon aging at 80 °C for 2 h and kept in a desiccator until use. All chemicals were used as purchased (see SI for details of Reagents and Materials).

A PDMS plate with six microchannels was designed. The channel dimensions were approximately 15 mm in length, 1 mm in width, and 65 μm in height (see SI for details of the preparation of the PDMS microchannel plate). Finally, the PDMS microchannel plate was tightly bonded onto the AuNPs@FPSF/ITO glass *via* plasma activation to ensure leakage-free flow operation of the HMC. Before use, the HMC was degassed in a vacuum chamber for 1 h.

2.2. Fabrication of the EIMR

Initially, the DNA aptamer TBA_{15} was infused into the channels of the HMC and immobilized on the AuNPs@FPSF/ITO glass *via* Au–S bond. The disulfide bond of TBA_{15} was reduced by incubating TBA_{15} with tris(2-carboxyethyl) phosphine hydrochloride (TCEP) for 0.5 h with the TBA_{15}-to-TCEP volume ratio of 40 : 1. TBA_{15} (15 μM) dissolved in Tris-EDTA buffer was pumped into the channels sequentially for 15 min at a flow rate of 0.5 μL min^{-1} and incubated for 16 h at 4 °C. To prevent nonspecific adsorption, 0.1% BSA buffer (1 mg mL^{-1}) was infused at a flow rate of 1 μL min^{-1} for 10 min and incubated for 0.5 h at 4 °C. The BSA solution was removed *via* vacuum suction, and the channels were rinsed with 1× PBS for 10 min at a flow rate of 1 μL min^{-1}. Subsequently, thrombin (20 U mL^{-1}) was infused into the channels for 10 min at a flow rate of 0.5 μL min^{-1} and incubated for 1 h at 25 °C away from light. The channels were then washed with the BSA solution followed by 1× PBS.

2.3. Determination of thrombin activity and screening of inhibitor using the EIMR

The activity of thrombin immobilized in the EIMR was determined *via* MALDI MS. The fluorescence substrate (30 μM, FITC-GC-11 NH_2) dissolved in acetonitrile/water (1 : 4, v/v) was

pumped into the channels at a flow rate of 0.5 μL min^{-1} until the channels were filled, followed by incubation for 0.5 h at 37 °C.

For thrombin inhibitor screening, argatroban or herbal extract solutions were infused into the channels for 0.5 h at a flow rate of 0.5 μL min^{-1} and incubated for 0.5 h at 37 °C, and then, the channels were washed with deionized water for 10 min at a flow rate of 1 μL min^{-1}. Afterward, 30 μM of FITC-GC-11 NH_2 was infused into the channels at a flow rate of 0.5 μL min^{-1} until the channels were filled, followed by incubation for 0.5 h at 37 °C. The enzymatic reaction in the channels was monitored *in situ via* fluorescence microscopy, and the fluorescence intensity was quantified using the ImageJ software. After the enzymatic reaction, the channels were completely dried at room temperature, and the PDMS plate was removed. The AuNPs@FPSF/ITO glass was sprayed with a MALDI matrix using a laboratory-constructed electro-sprayer and directly subjected to MALDI MS analysis.

2.4. Validation of the *in vitro* activity of potential thrombin inhibitors

80 μL of thrombin (20 U mL^{-1}), 20 μL of potential inhibitors at different concentrations (from 10 μM to 100 μM), and 20 μL of thrombin chromogenic substrate S-2238 (2 mM) were sequentially added to a 96-well plate. The mixed solution was shaken and incubated at 37 °C for 15 min, and absorbance was measured at 405 nm using a microplate reader. All measurements were performed in triplicate.

3. Results and discussion

3.1. Fabrication and characterization of the EIMR

As shown in Fig. 1A, the EIMR was developed based on an HMC. AuNPs@FPSF coatings were synthesized *in situ* for thrombin immobilization *via* three successive steps: growing a porous silica film using the Stöber-solution growth approach, functionalizing the porous silica film with R_4N^+ moieties, and reducing $[AuCl_4]^-$ by $NaBH_4$. Due to their good stability and biocompatibility, AuNPs were selected for the covalent-bonded immobilization of the thrombin DNA aptamer TBA_{15}. The entire synthesis procedure is simple, cost-effective, and does not require sophisticated facilities and conditions. The HRTEM and EDS were used to characterize the morphology and microstructure of the AuNPs@FPSF coatings. The HRTEM image shows that the structure of the coating is intact, and AuNPs are distributed uniformly in silica nanochannels without aggregation (Fig. 1B and C). The high density and uniform dispersion of AuNPs were mainly attributed to a facile and effective post-grafting with TMAC, which possesses a strong electrostatic interaction with $AuCl_4^-$.[29] EDS elemental maps reveal the spatial distribution of silicon (Si), oxygen (O), and gold (Au) species across the substrate surface, providing evidence for the successful fabrication of porous silica films with subsequent site-specific immobilization of AuNPs (Fig. 1D).

An aptamer-based EIMR demonstrates significant potential in enzyme immobilization applications owing to its unique advantages such as target-specific recognition, native confor-

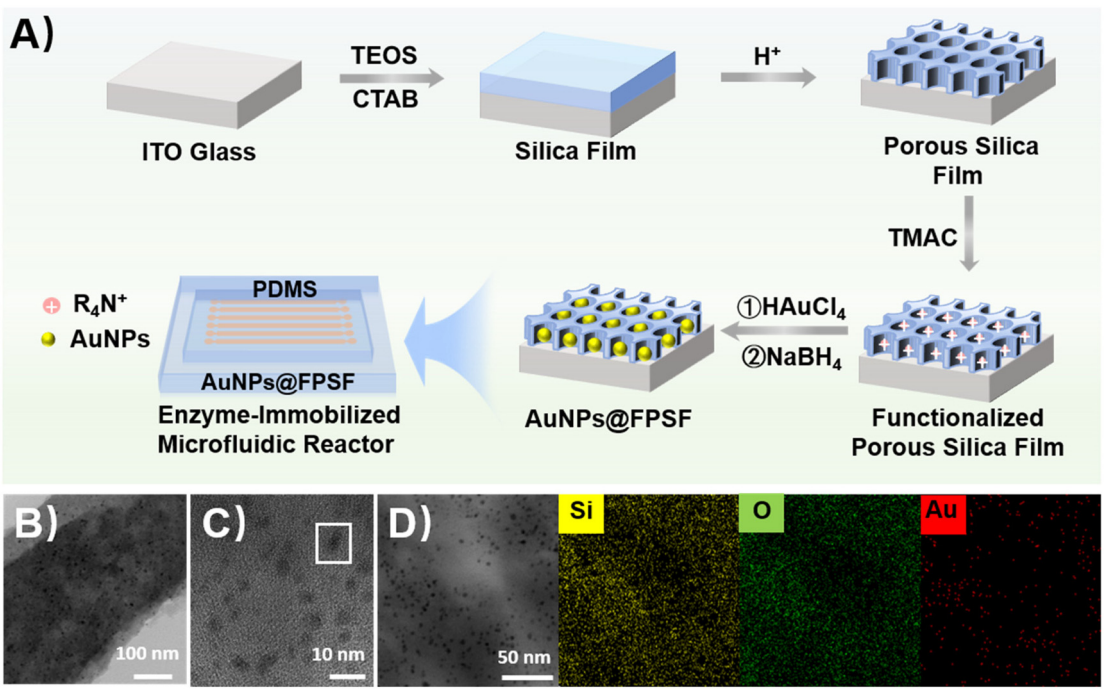

Fig. 1 (A) Fabrication of the EIMR based on an AuNPs@FPSF/ITO glass-six-channel PDMS hybrid microfluidic chip. (B) HRTEM image of AuNPs@FPSF. (C) HRTEM image of AuNPs. The black dot marked by the white box represents an AuNP immobilized on a functionalized porous silica film. (D) HRTEM-EDS images of Si (yellow), O (green), and Au (red) in AuNPs@FPSF.

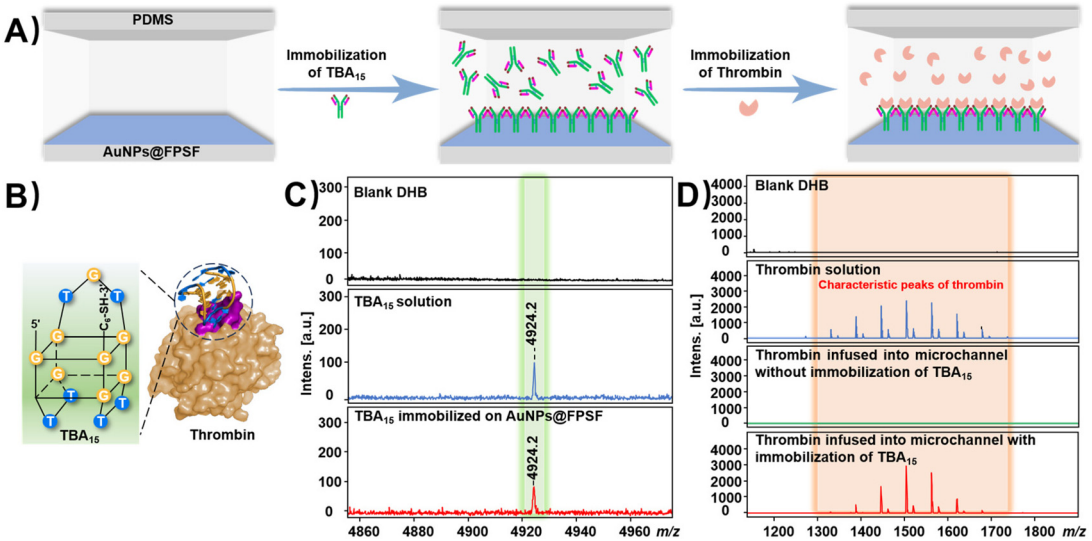

Fig. 2 (A) Schematic depicting the immobilization of thrombin in the EIMR. (B) Schematic of the binding between TBA_{15} and thrombin. (C) MALDI mass spectra of blank DHB (black line), TBA_{15} (blue line), and TBA_{15} immobilized on the AuNPs@FPSF/ITO glass (red line). (D) MALDI mass spectra of blank DHB (black line), thrombin (blue line), and thrombin infused into the channel without (green line) and with (red line) immobilization of TBA_{15} on the AuNPs@FPSF/ITO glass, respectively.

mation preservation, high binding affinity, and directional immobilization to maintain active sites.[30,31] Thrombin was subsequently immobilized in the channels using the DNA aptamer TBA_{15} to achieve an EIMR, which could be integrated with fluorescence and MALDI MS for determining thrombin activity and *in situ* screening of potential thrombin inhibitors from complex herbal extracts. TBA_{15} is a 15-base-long functional single-stranded DNA aptamer with an SH-C_6 oligo at 3′ termini, which can bind to the fibrinogen-recognition exosite of thrombin. TBA_{15} was immobilized on the AuNPs@FPSF/ITO glass through the Au–S bond (Fig. 2A and B), and MALDI MS was used to evaluate its immobilization. As shown in Fig. 2C, TBA_{15} can be detected in the channels ($[M + H]^+$, *m*/*z* 4924.2). After infusing thrombin into the channels, the characteristic peaks of thrombin with high MS signal intensity were detected (Fig. 2D). As expected, no characteristic thrombin peaks were detected in the channel without immobilization of TBA_{15} on AuNPs@FPSF. These results demonstrated that there was no non-specific adsorption of AuNPs@FPSF to thrombin and that TBA_{15} could strongly hold the thrombin during fluid flow.

3.2. Feasibility testing of the EIMR for thrombin activity assay

The activity of immobilized thrombin was first assessed for subsequent applications. The customized fluorescent substrate FITC-GC-11 NH_2 was synthesized for characterizing and monitoring thrombin activity. The identity of FITC-GC-11 NH_2 was first confirmed *via* MALDI MS and displayed molecular ions at *m*/*z* 1537.4 ($[M + H]^+$) (Fig. S1). The reaction of thrombin with its substrate could be monitored in real-time *via* fluorescence microscopy due to the introduction of a fluorescent tag (Fig. 3A). As shown in Fig. 3B, compared with the blank channel infused with FITC-GC-11 NH_2, the fluorescence intensity obtained from the TBA_{15}-immobilized channel significantly increased after sequential infusion of thrombin and FITC-GC-11 NH_2, which was mainly due to the thrombin-catalyzed hydrolysis resulting in an aggregation-induced emission effect, and thus improved the fluorescence detection sensitivity. Subsequently, the PDMS plate was removed, and the AuNPs@FPSF/ITO glass was sprayed with DHB matrix for MALDI MS analysis (Fig. 3C). The enzymatic hydrolysate was identified and quantified by MALDI MS to determine the thrombin activity. A peak at *m*/*z* 992.4 was observed in the MALDI mass spectrum after the infusion of FITC-GC-11 NH_2. Further analysis showed that the peak at *m*/*z* 992.4 was attributed to the peptide fragment FITC-Gly-D-Phe-Pip-Arg, generated by thrombin cleavage of Arg-Ser (Fig. S2). The identity of FITC-Gly-D-Phe-Pip-Arg was confirmed by comparing it with the MALDI MS/MS spectrum of the reference standard (Fig. S3). Therefore, the thrombin immobilized in the microfluidic reactor remained active and could *in situ* cleave FITC-GC-11 NH_2 in the EIMR. The fluorescence intensity and MS S/N ratio of the enzymatic hydrolysate FITC-Gly-D-Phe-Pip-Arg were used to further determine the optimal infusion time of thrombin and the substrate concentration. As shown in Fig. S4A and B, the fluorescence intensity and MS S/N ratio of the enzymatic hydrolysate increased with the infusion period ranging from 0 to 60 min, and thus, the optimal infusion time for thrombin immobilization was set to 60 min. Moreover, the optimal concentration of the fluorescent substrate was determined (Fig. S4C and D). The fluorescence intensity and MS S/N ratio of the enzymatic hydrolysate increased with the concentration of the substrate in the range of 0–30 μM, and no significant increase was observed over 30 μM. Therefore, 30 μM of the substrate was used for subsequent experiments.

The K_m of thrombin for FITC-GC-11 NH_2 was determined by measuring the amount of enzymatic hydrolysate *via* MALDI

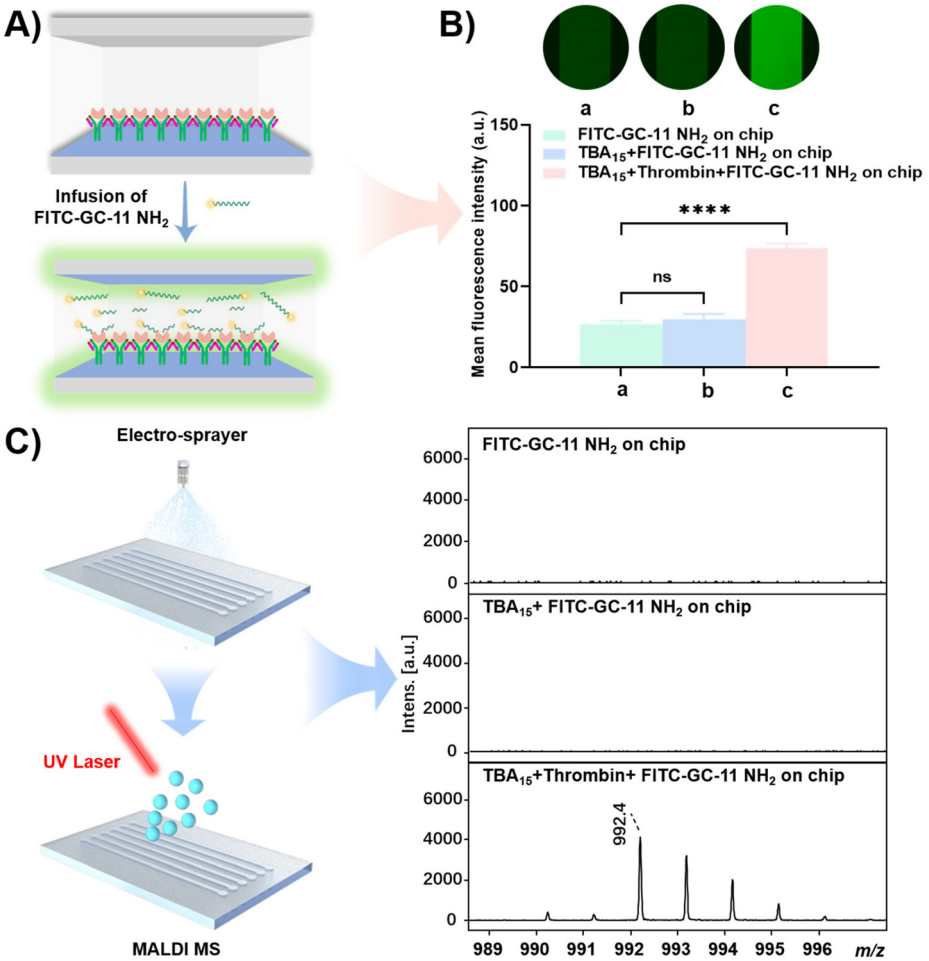

Fig. 3 (A) Experimental workflow for monitoring the activity of thrombin. (B) Mean fluorescence intensities and (C) MALDI mass spectra obtained from different channels. (a) Channel infused with FITC-GC-11 NH_2, (b) TBA_{15}-immobilized channel infused with FITC-GC-11 NH_2, and (c) TBA_{15}-immobilized channel sequentially infused with thrombin and FITC-GC-11 NH_2. Error bars correspond to the standard deviation of fluorescence intensities obtained from three positions of one channel. ns: no significant difference, ****$p < 0.0001$.

MS under the optimal conditions described above. The calibration curve was constructed by plotting the average MS S/N ratio of $[FITC\text{-}Gly\text{-}D\text{-}Phe\text{-}Pip\text{-}Arg + H]^+$ against the concentration of FITC-Gly-D-Phe-Pip-Arg. As shown in Fig. 4A, the MALDI MS results exhibited ideal linearity in the range of 1–50 μM with R^2 = 0.9912. Different amounts of FITC-GC-11 NH_2, ranging from 5 to 30 μM, were then incubated with 20 U mL^{-1} thrombin for the calculation of K_m (Fig. 4B). The K_m value of thrombin for FITC-GC-11 NH_2 was 2.6×10^{-5} M, showing good agreement with the previous study results.[32] Therefore, the developed EIMR in this work was reliable for determining thrombin activity.

3.3. Reproducibility testing of EIMR

The reproducibility across different channels and reactors was evaluated to confirm the reliability of the developed EIMR. The mean fluorescence intensity measured after enzymatic hydrolysis from three channels in one reactor was 54.1 ± 1.9, and the MS S/N ratio of the enzymatic hydrolysate measured from ten spots in one channel was 543.6 ± 5.3 (Fig. 4C–D and Table S1). Moreover, in Fig. 4C–D and Table S2, the fluorescence intensity measured after enzymatic hydrolysis from one channel of three reactors was 54.0 ± 0.8, and the MS S/N ratio of the enzymatic hydrolysate measured from ten spots from one channel of three reactors was 533.6 ± 2.3. Overall, the EIMR showed satisfactory reproducibility from channel-to-channel (RSD ≤ 9%) (Table S1) and reactor-to-reactor (RSD ≤ 10%) (Table S2).

3.4. Evaluation of the aptamer specificity and quantitative ability of EIMR

Quantitative detection of thrombin activity is useful for the early diagnosis of cardiovascular diseases and monitoring of anticoagulation therapy and postoperative coagulation status in patients.[33] To further demonstrate the performance of EIMR in the measurement of thrombin activity in complex biological systems, brain thrombin activity was determined in a rat model of transient middle cerebral artery occlusion (tMCAO). Initially, lysozyme, pepsin, trypsin, and thrombin

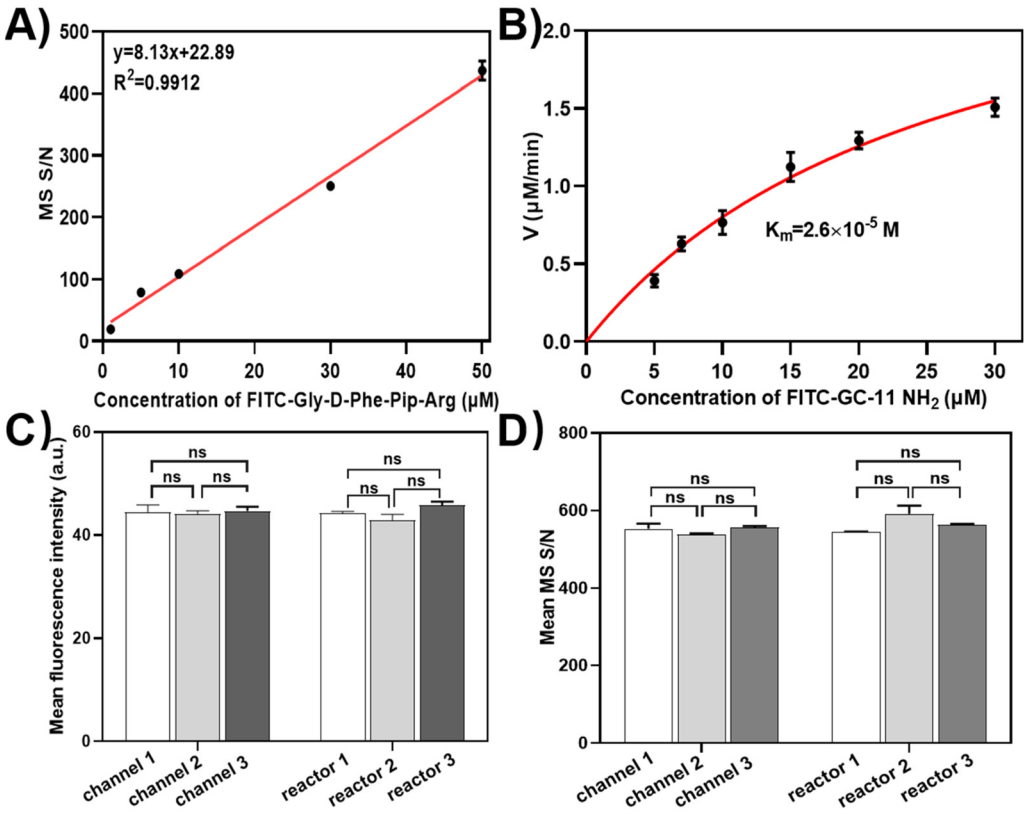

Fig. 4 (A) Quantitative calibration curve of FITC-Gly-D-Phe-Pip-Arg obtained by MALDI MS. Error bars correspond to the standard deviation of MS S/N ratios of FITC-Gly-D-Phe-Pip-Arg obtained from ten mass spectra. (B) Michaelis–Menten kinetic plot of the thrombin-catalyzed hydrolysis of FITC-GC-11 NH_2 determined by MALDI MS. The experiments were performed in triplicate. Error bars correspond to the standard deviation of three individual experiments. (C) Mean fluorescence intensity and (D) mean MS S/N ratio of FITC-Gly-D-Phe-Pip-Arg obtained from three channels in one reactor and three individual reactors, respectively. Error bars correspond to the standard deviation of fluorescence intensities obtained from three positions of one channel and the standard deviation of MS S/N ratios of FITC-Gly-D-Phe-Pip-Arg obtained from ten mass spectra of one channel. ns: no significant difference.

were selected to evaluate the selectivity of FITC-GC-11 NH_2 in a solution system. As shown in Fig. 5A, the fluorescence intensities increased significantly after the addition of thrombin and trypsin to the FITC-GC-11 NH_2 solution, while no significant changes in fluorescence intensities were observed after the addition of pepsin and lysozyme. This is because trypsin shares the same cleavage site as thrombin.[34] MALDI MS analysis further verified the fluorescence results. The enzymatic hydrolysate FITC-Gly-D-Phe-Pip-Arg was detected after the addition of thrombin and trypsin, indicating that both enzymes could cleave FITC-GC-11 NH_2 at Arg-Ser (Fig. 5B). Trypsin and thrombin were then used to test the specificity of TBA_{15} immobilized on the AuNPs@FPSF/ITO glass. As shown in Fig. 5C, no significant difference in fluorescence intensity was observed between the channels sequentially infused with trypsin and FITC-GC-11 NH_2 and the channels infused with FITC-GC-11 NH_2, whereas the fluorescence intensities in the channels significantly increased after sequential infusion with thrombin and FITC-GC-11 NH_2. The MALDI MS results indicated that FITC-Gly-D-Phe-Pip-Arg was detected in the thrombin-infused channels, while FITC-Gly-D-Phe-Pip-Arg was not detected in the trypsin-infused channels (Fig. 5D). The results indicated that TBA_{15} could specifically bind to thrombin. Furthermore, the thrombin activities of the ischemic and contralateral hemispheres of tMCAO rats were determined using the developed EIMR. As shown in Fig. S5 and Table S3, the thrombin activity in the ischemic hemisphere (right, 11 ± 1.3 mU mL^{-1}) was significantly higher than that in the contralateral hemisphere (left, 2.6 ± 0.8 mU mL^{-1}). The above results indicated that the developed EIMR has good specificity and quantitative ability for determining thrombin activity in complex biological samples.

3.5. Screening and identification of natural thrombin inhibitors from herbal extracts using the EIMR

Due to its satisfactory performance, the EIMR showed great potential for the screening of thrombin inhibitors from complex herbal extracts (Fig. 6A). Initially, the direct thrombin inhibitor argatroban was utilized to validate the feasibility of the EIMR. The fluorescence results indicated that the fluorescence intensity in the channel significantly decreased after the infusion of argatroban, whereas a strong fluorescence intensity was observed in the absence of argatroban (Fig. S6A). This result was further confirmed by the MALDI MS analysis, which demonstrated the pres-

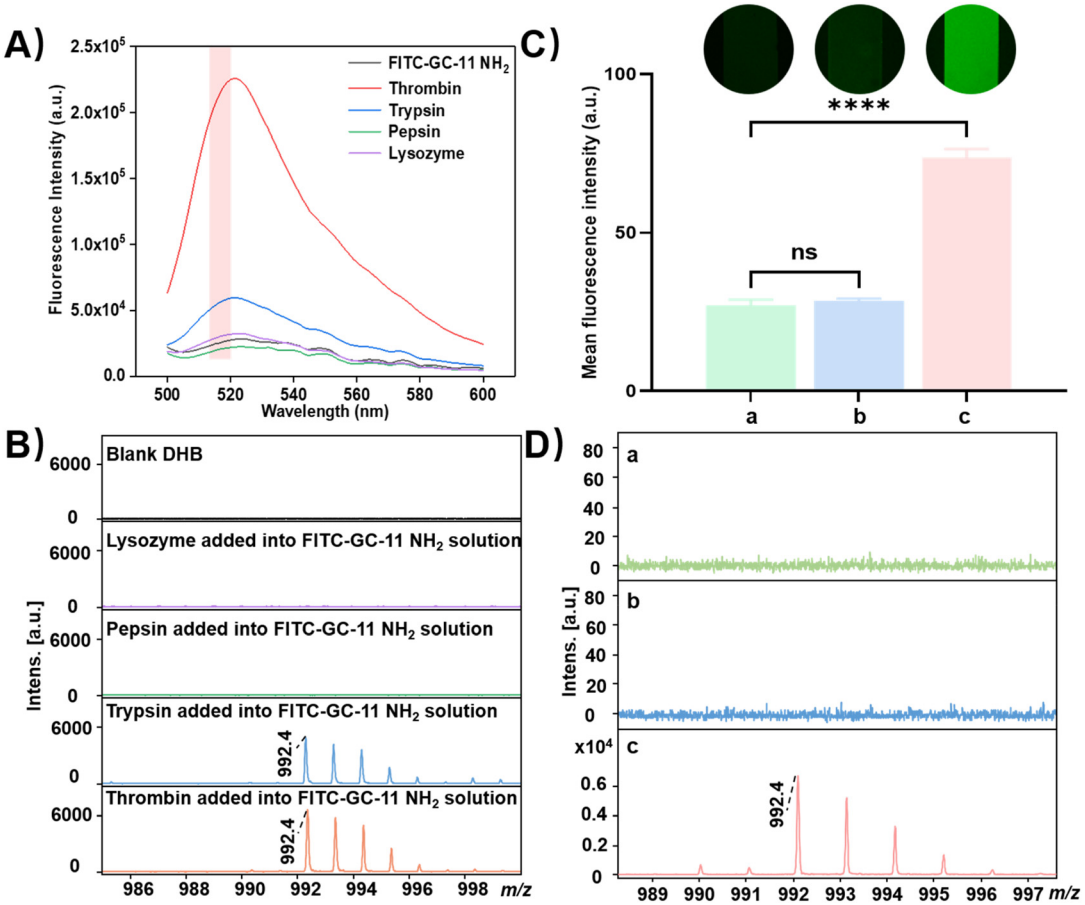

Fig. 5 (A) Evaluation of the selectivity of FITC-GC-11 NH_2 *via* fluorescence microscopy and (B) MALDI MS. (C) Mean fluorescence intensity and (D) MALDI mass spectra of FITC-Gly-D-Phe-Pip-Arg obtained from different channels infused with FITC-GC-11 NH_2: (a) blank channel and TBA_{15}-immobilized channel infused with (b) trypsin and (c) thrombin. Error bars correspond to the standard deviation of fluorescence intensities obtained from three positions of one channel. ns: no significant difference, ****$p < 0.0001$.

ence of both argatroban ($[M + H]^+$, *m/z* 509.1) and the substrate (*m/z* 1537.4) in the channels after the infusion of argatroban, whereas the MS signal of the enzymatic hydrolysate FITC-Gly-D-Phe-Pip-Arg (*m/z* 992.4) was not observed (Fig. S6B and D). As expected, FITC-Gly-D-Phe-Pip-Arg could be detected in channels without the infusion of argatroban.

Furthermore, the fabricated EIMR was used for screening potential thrombin inhibitors from complex herbal extracts. Five herbal extracts with potency in activating blood circulation and removing blood stasis were selected to evaluate their thrombin inhibitory activities and screen potential natural thrombin inhibitors, including the Carthami Flos extract (CFE),[35] Coptidis Rhizoma extract (CRE),[36] Polygalae Radix extract (PRE),[37] Ligustri Lucidi Fructus extract (LLFE),[38] and Hyperici Perforati Herba extract (HPHE).[39] As shown in Fig. 6B, compared with the channel without the infusion of inhibitors, the fluorescence intensity of the channels significantly decreased after the infusion of CFE, CRE, PRE, HPHE, and LLFE, indicating that the five herbal extracts have potential anti-thrombin effects. MALDI MS was further used to detect the enzymatic hydrolysate FITC-Gly-D-Phe-Pip-Arg and identify potential thrombin inhibitors in herbal extracts (Fig. 6B). The MS signal intensity of FITC-Gly-D-Phe-Pip-Arg significantly decreased in the channels after the infusion of five herbal extracts, consistent with the fluorescence results. To further screen the compounds with a binding affinity towards thrombin, MALDI MS analysis was conducted on the EIMR. As shown in Fig. 6C, eight peaks were detected in both raw herbal extracts and the EIMR after the infusion of five herbal extracts. By comparing the MALDI MS/MS spectra of detected peaks with reference standards, eight natural products were identified as luteolin ($[M + H]^+$, *m/z* 287.1) and baicalin ($[M + H]^+$, *m/z* 447.1) from LLFE, quercetin ($[M + H]^+$, *m/z* 303.1) and hyperoside ($[M + Na]^+$, *m/z* 487.1) from HPHE, berberine ($[M]^+$, *m/z* 336.1) from CRE, sibiricaxanthone A ($[M + Na]^+$, *m/z* 561.1) and tenuifolin ($[M + Na]^+$, *m/z* 703.1) from PRE, and hydroxysafflor yellow A ($[M - H]^-$, *m/z* 611.1) from CFE (Fig. S7).

3.6. Validation of the *in vitro* activity of potential thrombin inhibitors

Subsequently, the thrombin chromogenic substrate S-2238 was used to validate the inhibitory effect of eight compounds on thrombin. As shown in Fig. S8, all eight compounds showed

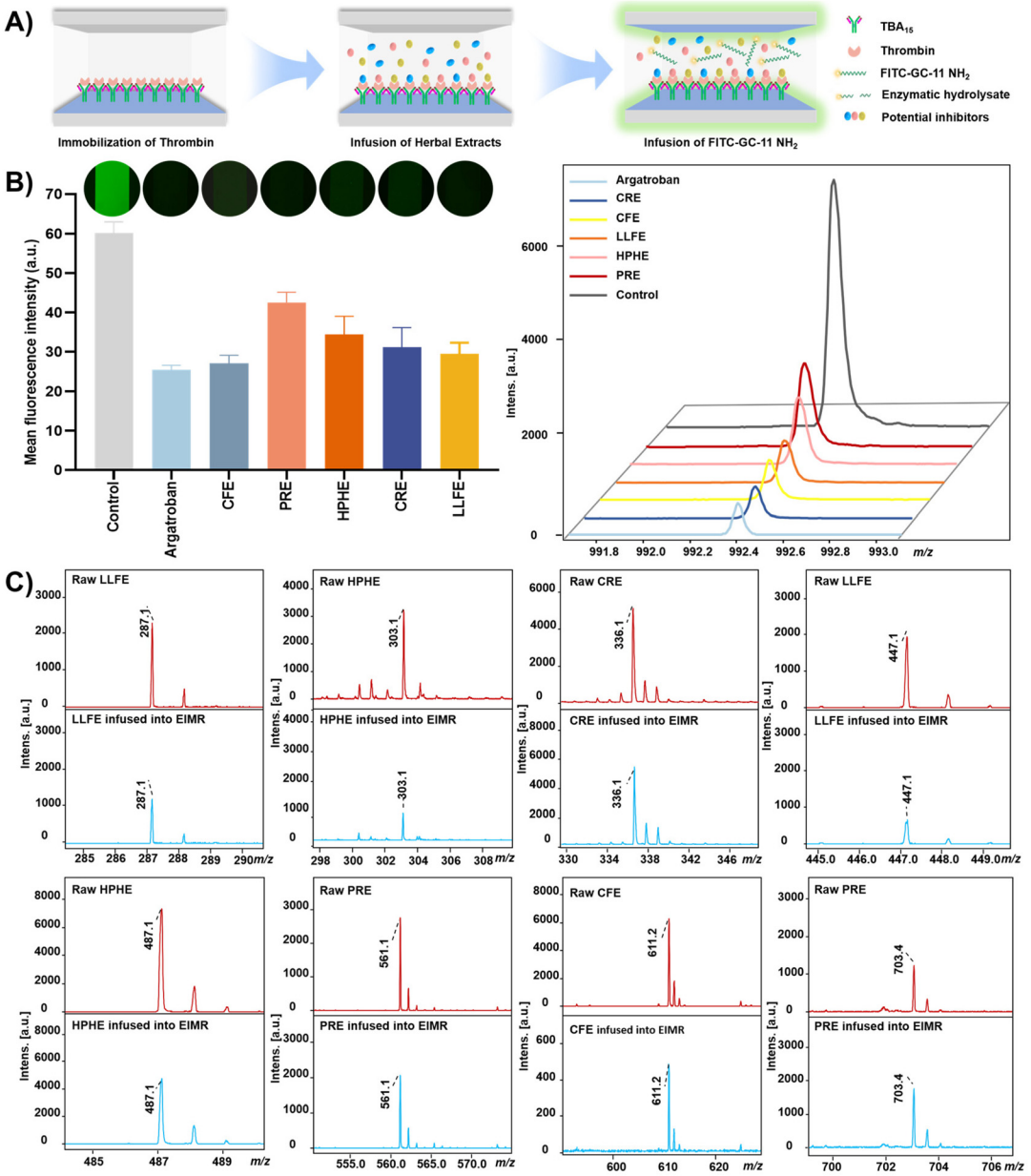

Fig. 6 (A) Schematic of the thrombin inhibitor screening from five herbal extracts using the EIMR. (B) Mean fluorescence intensity and corresponding fluorescence images and representative MALDI mass spectra of FITC-Gly-D-Phe-Pip-Arg obtained from different channels after the infusion of argatroban and five herbal extracts. Error bars correspond to the standard deviation of fluorescence intensities obtained from three positions of one channel. (C) MALDI mass spectra obtained from raw herbal extracts and the EIMR. CFE: carthami flos extract, PRE: polygalae radix extract, HPHE: hyperici perforati herba extract, CRE: coptidis rhizoma extract, LLFE: ligustri lucidi fructus extract.

potential anti-thrombin activity. Among them, luteolin, quercetin, berberine, baicalein, and hypericin showed good anti-thrombin activity, consistent with previous studies.[28,40,41] However, the thrombin inhibitory activities of hydroxysafflor yellow A, tenuifolin, and sibiricaxanthone A were barely reported in the literature. Therefore, the IC_{50} values of hydroxysafflor yellow A, tenuifolin, and sibiricaxanthone A for the inhibition of thrombin were further determined *via* MALDI MS (Fig. S9). The concentration-response curves of three candidate thrombin inhibitors were generated, and the IC_{50} values of hydroxysafflor yellow A, tenuifolin, and sibiricaxanthone A were 34.97 μM, 9.64 μM, and 12.55 μM, respectively.

4. Conclusions

In summary, an enzyme-immobilized microfluidic reactor (EIMR) integrated with two detection modalities, fluorescence and MALDI MS, was developed to determine thrombin activity in biological samples and to *in situ* screen and identify poten-

tial natural thrombin inhibitors from complex herbal extracts. The developed EIMR showed high tolerance towards interferences from complex herbal extracts and could be used for reactions in a micromixing channel with less reagent consumption. The inhibitory effects of five herbal extracts on thrombin were evaluated using the EIMR. More importantly, eight natural products with strong anti-thrombin activity were discovered and identified from five herbal extracts, among which the IC_{50} values of hydroxysafflor yellow A, tenuifolin, and sibiricaxanthone A were below 35 μM. Overall, the developed EIMR possesses certain advantages, such as miniaturization, integration, and portability, and provides a promising screening platform for identifying drug candidates from natural sources.

Author contributions

Xian-Na Wang, Yahui Song, Ji Zhang, Rui-Ping Song, and Weiwei Tang: investigation, methodology, data curation, writing – original draft. Bin Li: conceptualization, funding acquisition, supervision, writing – review & editing.

Conflicts of interest

The authors declare that they have no known competing financial interests or personal relationships that could have appeared to influence the work reported in this paper.

Data availability

The data supporting this article has been included as part of the supplementary information (SI). Supplementary information is available. See DOI: https://doi.org/10.1039/d5an01290b.

Acknowledgements

This work was supported by the National Natural Science Foundation of China (No. 82374028) and the 111 project (B16046). The content is solely the responsibility of the authors and does not necessarily represent the official views of the funding agencies.

References

1 I. Tzoulaki, P. Elliott, V. Kontis and M. Ezzati, Worldwide Exposures to Cardiovascular Risk Factors and Associated Health Effects: Current Knowledge and Data Gaps, *Circulation*, 2016, **133**, 2314–2333.
2 C. Negrier, M. Shima and M. Hoffman, The central role of thrombin in bleeding disorders, *Blood Rev.*, 2019, **38**, 100582.
3 S. Yu, J. Liu, L. Li, K. Ma, J. Kong and X. Zhang, An electrochemical biosensor for the amplification of thrombin activity by perylene-mediated photoinitiated polymerization, *Anal. Chim. Acta*, 2024, **1302**, 342494.
4 Y. Wang, J. Wang, R. Wang, Y. Liu, G. I. N. Waterhouse, X. Ding and V. Raghavan, Single aptamer hairpin DNA-based response system combined with COF-based signal amplification strategy for ultrasensitive detection of cancer-associated thrombin, *Chem. Eng. J.*, 2024, **489**, 151224.
5 K. E. Brummel, S. G. Paradis, S. Butenas and K. G. Mann, Thrombin functions during tissue factor-induced blood coagulation, *Blood*, 2002, **100**, 148–152.
6 S. Robert, J. Ghiotto, B. Pirotte, J.-L. David, B. Masereel, L. Pochet and J.-M. Dogné, Is thrombin generation the new rapid, reliable and relevant pharmacological tool for the development of anticoagulant drugs?, *Pharmacol. Res.*, 2009, **59**, 160–166.
7 D. Òªimen, N. Bereli, S. Günaydın and A. Denizli, Molecular imprinted nanoparticle assisted surface plasmon resonance biosensors for detection of thrombin, *Talanta*, 2022, **246**, 123484.
8 J. Wang, M. Song, C. Hu and K. Wu, Portable, Self-Powered, and Light-Addressable Photoelectrochemical Sensing Platforms Using pH Meter Readouts for High-Throughput Screening of Thrombin Inhibitor Drugs, *Anal. Chem.*, 2018, **90**, 9366–9373.
9 X. Feng, A. Sureda, S. Jafari, Z. Memariani, D. Tewari, G. Annunziata, L. Barrea, S. T. S. Hassan, K. Smejkal, M. Malanik, A. Sychrova, D. Barreca, L. Ziberna, M. F. Mahomoodally, G. Zengin, S. Xu, S. M. Nabavi and A. Z. Shen, Berberine in Cardiovascular and Metabolic Diseases: From Mechanisms to Therapeutics, *Theranostics*, 2019, **9**, 1923–1951.
10 H. Kuang, L. Kong, A. Hou, A. Yang and H. Jiang, A review of the botany, metabolites, pharmacology, toxicity, industrial applications, and processing of Polygalae Radix: the "key medicine for nourishing life", *Front. Pharmacol.*, 2024, **15**, 1450733.
11 M. Huang, X. Xie, R. Yuan, Q. Xin, S. Ma, H. Guo, Y. Miao, C. Hu, Y. Zhu and W. Cong, The multifaceted anti-atherosclerotic properties of herbal flavonoids: A comprehensive review, *Pharmacol. Res.*, 2025, **211**, 107551.
12 X. Hou, M. Sun, T. Bao, X. Xie, F. Wei and S. Wang, Recent advances in screening active components from natural products based on bioaffinity techniques, *Acta Pharm. Sin. B*, 2020, **10**, 1800–1813.
13 W. Hu, J. Hou, W. Liu, X. Gu, Y. Yang, H. Shang and M. Zhang, Online pharmaceutical process analysis of Chinese medicine using a miniature mass spectrometer: Extraction of active ingredients as an example, *J. Pharm. Anal.*, 2023, **13**, 535–543.
14 J. Meng, Q. Li, Z. Cao, D. Gu, Y. Wang, Y. Zhang, Y. Wang, Y. Yang and F. He, Rapid screening and separation of active compounds against α-amylase from Toona sinensis by ligand fishing and high-speed counter-current chromatography, *Int. J. Biol. Macromol.*, 2021, **174**, 270–277.

15 S. Guo, S. Wang, J. Meng, D. Gu and Y. Yang, Immobilized enzyme for screening and identification of anti-diabetic components from natural products by ligand fishing, *Crit. Rev. Biotechnol.*, 2023, **43**, 242–257.
16 M. Wang, W. Qi, R. Su and Z. He, Advances in carrier-bound and carrier-free immobilized nanobiocatalysts, *Chem. Eng. Sci.*, 2015, **135**, 21–32.
17 R. C. Rodrigues, Á. Berenguer-Murcia, D. Carballares, R. Morellon-Sterling and R. Fernandez-Lafuente, Stabilization of enzymes via immobilization: Multipoint covalent attachment and other stabilization strategies, *Biotechnol. Adv.*, 2021, **52**, 107821.
18 B. H. Weigl and P. Yager, Microfluidics - Microfluidic diffusion-based separation and detection, *Science*, 1999, **283**, 346–347.
19 L. Y. Yeo, H. C. Chang, P. P. Chan and J. R. Friend, Microfluidic devices for bioapplications, *Small*, 2011, **7**, 12–48.
20 M. Breitfeld, C. L. Dietsche, M. A. Saucedo-Espinosa, S. F. Berlanda and P. S. Dittrich, Ultrafast Formation of Microdroplet Arrays with Chemical Gradients for Label-Free Determination of Enzymatic Reaction Kinetics, *Small*, 2025, e2410275.
21 T. Wang, J. Ma, G. Zhu, Y. Shan, Z. Liang, L. Zhang and Y. Zhang, Integration of capillary isoelectric focusing with monolithic immobilized pH gradient, immobilized trypsin microreactor and capillary zone electrophoresis for on-line protein analysis, *J. Sep. Sci.*, 2010, **33**, 3194–3200.
22 K. Meller, M. Szumski and B. Buszewski, Microfluidic reactors with immobilized enzymes—Characterization, dividing, perspectives, *Sens. Actuators, B*, 2017, **244**, 84–106.
23 A. Šalić, A. Tušek and B. Zelić, Application of microreactors in medicine and biomedicine, *J. Appl. Biomed.*, 2012, **10**, 137–153.
24 J. Michelena, A. Lezaja, F. Teloni, T. Schmid, R. Imhof and M. Altmeyer, Analysis of PARP inhibitor toxicity by multidimensional fluorescence microscopy reveals mechanisms of sensitivity and resistance, *Nat. Commun.*, 2018, **9**, 2678.
25 X. Yu, W. Yu, X. Zhang, Y. Wang, S. Wang and H. Zhai, Simultaneous determination of flavonoids and anthraquinones in honey by using SPE-CE-LIF, *Anal. Biochem.*, 2021, **631**, 114373.
26 S. Sun, W. Tang and B. Li, Authentication of Single Herbal Powders Enabled by Microscopy-Guided In Situ Autosampling Combined with Matrix-Assisted Laser Desorption/Ionization Mass Spectrometry, *Anal. Chem.*, 2023, **95**, 7512–7518.
27 H.-P. Chen and H.-H. Hsiao, Facile fabrication of the immuno-MALDI-MS chip for the enrichment of abused drug in human urine integrated with MALDI-MS analysis, *Anal. Chim. Acta*, 2024, **1329**, 343224.
28 X. N. Wang, Y. Song, W. Tang, P. Li and B. Li, Integration of fluorescence and MALDI imaging for microfluidic chip-based screening of potential thrombin inhibitors from natural products, *Biosens. Bioelectron.*, 2023, **237**, 115527.
29 Z.-M. Lyu, X.-L. Zhou, X.-N. Wang, P. Li, L. Xu and E. H. Liu, Miniaturized electrochemiluminescent biochip prepared on gold nanoparticles-loaded mesoporous silica film for visual detection of hydrogen peroxide released from living cells, *Sens. Actuators, B*, 2019, **284**, 437–443.
30 M. Debiais, A. Lelievre, M. Smietana and S. Müller, Splitting aptamers and nucleic acid enzymes for the development of advanced biosensors, *Nucleic Acids Res.*, 2020, **48**, 3400–3422.
31 M. Song, X. Wu, K. Fan, G. Qiu, X. Zhang, Z. Wu, S. Wang and W. Wen, A dual-switch electrochemical aptasensor for label-free detection of thrombin and ATP based on split aptamers, *Anal. Chim. Acta*, 2025, **1335**, 343441.
32 W. Tang, A. Gordon, H. Y. Wang, P. Li, J. Chen and B. Li, Development of MALDI MS peptide array for thrombin inhibitor screening, *Talanta*, 2021, **226**, 122129.
33 C. Han, X. Yuan, Z. Shen, Y. Xiao, X. Wang, M. Khan, S. Liu, W. Li, Q. Hu and W. Wu, A paper-based lateral flow sensor for the detection of thrombin and its inhibitors, *Anal. Chim. Acta*, 2022, **1205**, 339756.
34 A. P. Lobo, J. D. Wos, S. M. Yu and W. B. Lawson, Active site studies of human thrombin and bovine trypsin: peptide substrates, *Arch. Biochem. Biophys.*, 1976, **177**, 235–244.
35 G. Fan, M. Liu, J. Liu, Y. Huang and W. Mu, Traditional Chinese medicines treat ischemic stroke and their main bioactive constituents and mechanisms, *Phytother. Res.*, 2024, **38**, 411–453.
36 N. Li, G. Zhang, Y. Liu, L. Sun, X. Zhao, L. Ding, Y. Liu, M. Wang and X. Ren, A Natural Self-Assembled Gel-Sponge with Hierarchical Porous Structure for Rapid Hemostasis and Antibacterial, *Adv. Healthcare Mater.*, 2023, **12**, e2301465.
37 M. Gao, J. Lan, B. Bao, W. Yao, Y. Cao, M. Shan, F. Cheng, P. Chen and L. Zhang, Effects of carbonized process on quality control, chemical composition and pharmacology of Typhae Pollen: A review, *J. Ethnopharmacol.*, 2021, **270**, 113774.
38 M. Cao, J. Wu, Y. Peng, B. Dong, Y. Jiang, C. Hu, L. Yu and Z. Chen, Ligustri Lucidi Fructus, a traditional Chinese Medicine: Comprehensive review of botany, traditional uses, chemical composition, pharmacology, and toxicity, *J. Ethnopharmacol.*, 2023, **301**, 115789.
39 L. H. Wei, T. R. Chen, H. B. Fang, Q. Jin, S. J. Zhang, J. Hou, Y. Yu, T. Y. Dou, Y. F. Cao, W. Z. Guo and G. B. Ge, Natural constituents of St. John's Wort inhibit the proteolytic activity of human thrombin, *Int. J. Biol. Macromol.*, 2019, **134**, 622–630.
40 P. Saravia-Otten, R. Hernández, N. Marroquín, J. A. Pereañez, L. M. Preciado, A. Vásquez, G. García, F. Nave, L. Rochac, V. Genovez, M. Mérida, S. M. Cruz, N. Orozco, A. Cáceres and J. M. Gutiérrez, Inhibition of enzymatic activities of Bothrops asper snake venom and docking analysis of compounds from plants used in Central America to treat snakebite envenoming, *J. Ethnopharmacol.*, 2022, **283**, 114710.
41 X. Wang, Y. Zhang, Y. Yang, X. Wu, H. Fan and Y. Qiao, Identification of berberine as a direct thrombin inhibitor from traditional Chinese medicine through structural, functional and binding studies, *Sci. Rep.*, 2017, **7**, 44040.

